Exchange bias and surface effects in bimagnetic CoO-core/$Co_{0.5}Ni_{0.5}Fe_2O_4$-shell nanoparticles

Gabriel Lavorato,[1] Elin Winkler,[1,*] Alberto Ghirri,[2] Enio Lima, Jr.,[1] Davide Peddis,[3] Horacio E. Troiani,[1] Dino Fiorani,[3] Elisabetta Agostinelli,[3] Daniele Rinaldi,[4] and Roberto D. Zysler[1]

[1]*Centro Atómico Bariloche, CNEA-CONICET, 8400 S.C. de Bariloche, Río Negro, Argentina*

[2]*Istituto Nanoscienze, CNR, via Campi 213/a, I-41125 Modena, Italy*

[3]*Istituto di Struttura della Materia, CNR, Area della Ricerca di Roma 1, C.P. 10, I-00015 Monterotondo Stazione, Rome, Italy*

[4]*Dipartimento SIMAU, Universitá Politecnica delle Marche via Brecce Bianche, I-60131 Ancona, Italy*

(Received 5 June 2016; revised manuscript received 10 August 2016; published 30 August 2016)

Bimagnetic nanoparticles have been proposed for the design of new materials with controlled properties, which requires a comprehensive investigation of their magnetic behavior due to multiple effects arising from their complex structure. In this work we fabricated bimagnetic core/shell nanoparticles formed by an ∼3-nm antiferromagnetic (AFM) CoO core encapsulated within an ∼1.5-nm ferrimagnetic (FiM) $Co_{0.5}Ni_{0.5}Fe_2O_4$ shell, aiming at studying the enhancement of the magnetic anisotropy and the surface effects of a ferrimagnetic oxide shell. The magnetic properties of as-synthesized and annealed samples were analyzed by ac and dc magnetization measurements. The results indicate that the magnetic response of the as-synthesized particles is governed by the superparamagnetic behavior of the interacting nanoaggregates of spins that constitute the disordered ferrimagnetic shell, whose total moments block at $\langle T_B \rangle = 49$ K and collectively freeze in a superspin-glass-type state at $\langle T_g \rangle = 3$ K. On the other hand, annealed nanoparticles are superparamagnetic at room temperature and behave as an exchange-coupled system below the blocking temperature $\langle T_B \rangle = 70$ K, with enhanced coercivity $H_C(10\text{ K}) \sim 14.6$ kOe and exchange bias field $H_{EB}(10\text{ K}) \sim 2.3$ kOe, compared with the as-synthesized system where $H_C(10\text{ K}) \sim 5.5$ kOe and $H_{EB}(10\text{ K}) \sim 0.8$ kOe. Our results, interpreted using different models for thermally activated and surface relaxation processes, can help clarify the complex magnetic behavior of many core/shell and hollow nanoparticle systems.

DOI: 10.1103/PhysRevB.94.054432

I. INTRODUCTION

The search for control and manipulation of materials' physical properties has led to the design and manufacture of increasingly complex nanostructures [1,2]. Depending on the field of application, the magnetic characteristics required for a magnetic nanoparticle system can sensibly change. For example, to develop new permanent magnets and new materials for high-density data storage, novel nanoparticle systems with enhanced effective magnetic anisotropy [3], tuned magnetotransport properties [4], improved squareness [5,6], and increased thermal stability of the magnetic moment [7] are needed; on the other hand, biomedical applications, such as hyperthermia or contrast agents for magnetic resonance imaging, require biocompatible nanoparticles superparamagnetic at room temperature [8] and precise tuning of the magnetic properties for efficient heat induction [9,10]. Accordingly, the structural complexity of nanoparticles has also increased, and currently, the focus is on the design of core/shell structures that combine materials with different compositions [11], sizes [12], and anisotropies [13]. In this frame, antiferromagnetic (AFM), ferromagnetic (FM), and ferrimagnetic (FiM) materials can be arranged in various structures such as FM(FiM)/AFM core/shell [14], AFM/FiM inverted core/shell [15], or doubly inverted core/shell nanoparticles [16,17].

Although novel structures can be fabricated by finely tuning the synthesis methods, the increasing degree of microstructural complexity hinders the control of the properties because new effects such as stoichiometry gradient [18], interface diffusion [19], crystalline disorder, and/or surface magnetic disorder [20–23] are manifested. In this context, detailed studies of surface effects, interface-dependent properties, and magnetic interactions in bimagnetic nanoparticles are still lacking and represent an essential step to understand their static and dynamic magnetic response and how it is determined by the internal structure of the system.

In core/shell nanoparticles the crystalline order of the core phase is improved compared to the coating as the latter grows in less favorable conditions [24]. Therefore, inverted structure allows better control of the hard AFM phase quality and consequently optimizes the magnetic properties induced by the interface [16,17,20,21,25]. Here we investigate by means of dc magnetization and ac susceptibility measurements the magnetic properties of bimagnetic singly inverted core/shell nanoparticles. The particles are formed by hard AFM CoO ($T_{N-\text{Bulk}} \sim 290$ K) cores encapsulated in a FiM $Co_{0.5}Ni_{0.5}Fe_2O_4$ ($T_{C-\text{Bulk}} \sim 800$ K) shell.

The purpose of this work is to analyze the AFM/FiM coupling at the interface and its influence on the magnetic hardening of core/shell nanoparticles systems with different crystalline and magnetic disorder degrees. In this particular system the order degree can be controlled by thermal treatment, which increases the crystallinity of the AFM core and, as a consequence, improves the exchange coupling at the interface [26]. We found that while the magnetic behavior of the as-synthesized nanoparticles is governed by the dynamics of the magnetic moments of nanoaggregates of spins that form the highly disorder shell, which collectively freeze at low temperature, the magnetic properties of annealed nanoparticles are ruled by the AFM/FiM interface interaction, responsible

*winkler@cab.cnea.gov.ar

for the observation of exchange bias and for a remarkable anisotropy enhancement.

II. EXPERIMENTAL DETAILS

$CoO/Co_{0.5}Ni_{0.5}Fe_2O_4$ nanoparticles were fabricated by means of the thermal decomposition of metal acetylacetonates in diphenyl ether, assisted by oleic acid and oleylamine. In a typical synthesis the chemical reactives are mixed in a three-neck 500-mL flask with a reflux condenser, refrigerated with water, under N_2 atmosphere. To obtain CoO seeds, 4 mmol of $Co(acac)_2$, 8 mmol of oleic acid, 8 mmol of oleylamine, 2 mmol of 1,2-octanediol, and 235 mmol of diphenyl ether were mixed and heated to the reflux temperature (260 °C) at a fixed rate of 20 °C/min and kept at that temperature for 2 h. Once cooled to room temperature, 1.6 mmol of $Fe(acac)_3$, 0.4 mmol of $Co(acac)_2$, 0.4 mmol of $Ni(acac)_2$, 4 mmol of oleic acid, 4 mmol of oleylamine, and 79 mmol of diphenyl ether were added to the preparation. The solution was then reheated at a heating rate of 30 °C/min to the reflux temperature (260 °C) and kept at that temperature for 2 h in order to obtain core/shell nanoparticles. Subsequently, the mixture was washed several times by centrifugation (14 000 rpm/30 min) by adding an 8:1 mixture of ethanol and toluene. By evaporating the solvent a dry powder was obtained. In order to investigate the effects of a thermal treatment, a fraction of the resulting material was annealed at 300 °C for 2 h under air atmosphere, with a fixed heating rate of 2.5 °C/min. Both samples were redispersed with toluene in an epoxy resin in order to avoid the mechanical movement of the nanoparticles during the magnetic measurements. The amount of the residual organic mass from the synthesis was evaluated by a thermogravimetric analyzer (TGA, Shimadzu DTG-60H) by heating the samples up to 600 °C in air atmosphere with a fixed heating rate of 5 °C/min. For comparison, the same experiment was performed for oleic acid.

The structural characterization was performed by means of an x-ray diffractometer (XRD; PANAlytical X'Pert equipment with CuKα radiation) and a transmission electron microscope (TEM; Philips CM200, Ultra-Twin lens, operating at 200 kV). The crystalline structure and the morphology of the nanoparticles were investigated by analyzing x-ray diffractograms and bright-field, dark-field, and high-resolution TEM images. The magnetic characterization was performed using a superconducting quantum interference device (SQUID magnetometer, Quantum Design) with a maximum applied field of ±70 kOe. The temperature dependence of magnetization was evaluated by measuring zero-field-cooled (ZFC) and field-cooled (FC) curves between 5 and 330 K with an applied field of 50 Oe. The ac magnetic measurements were performed by a Quantum Design PPMS ac/dc magnetometer varying the frequency f in the range of 10 Hz to 10 kHz with a driving field $H_{ac} = 10$ Oe.

III. RESULTS AND DISCUSSION

Figure 1 shows the diffraction patterns for as-synthesized and annealed samples. The peaks were indexed with the diffraction positions of $Fm\bar{3}m$ rock salt and $Fd\bar{3}m$ spinel structures associated with CoO (JCPDS No. 43-1004) and

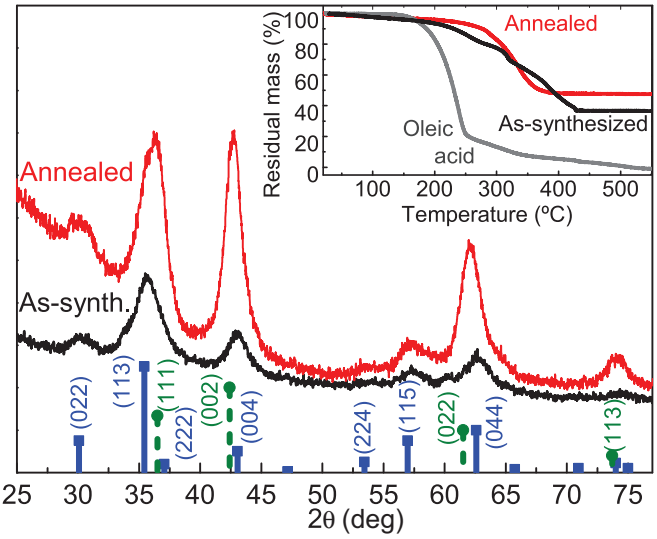

FIG. 1. X-ray diffraction patterns of as-synthesized and annealed $CoO/Co_{0.5}Ni_{0.5}Fe_2O_4$ nanoparticles. The positions of bulk CoO (dashed vertical lines) and $CoFe_2O_4$ (solid vertical lines) reflections are shown for comparison. The inset shows the thermogravimetric curves for both samples and oleic acid measured under air atmosphere.

$CoFe_2O_4$ (JCPDS No. 22-1086) bulk structures, also indicated in the graph. Unlike other core-shell nanoparticle systems where the as-synthesized sample presents excellent quality of the component phases [11,27,28], the CoO core is poorly crystalline. After the annealing, the crystalline order of the CoO phase improves, as observed from the comparison between the x-ray relative intensities of the spinel and rock-salt phases. This result highlights one of the advantages of inverted core/shell structures where the shell preserves the CoO core against oxidation, allowing a better crystalline order and better control of the magnetic order of the AFM phase [24,26].

The lattice parameter of the CoO phase is close to its bulk value (4.26 Å), while the lattice parameter of the spinel phase is 8.35(1) Å, in agreement with Ni-substituted $CoFe_2O_4$ since $a_{CoFe_2O_4} = 8.39$ Å and $a_{NiFe_2O_4} = 8.34$ Å [29]. The mean crystallite size D of both phases was analyzed with the Scherrer formula $D = K\lambda/\beta\cos(\theta)$, where K is a constant related to the shape of the nanocrystal (usually considered equal to 0.89), β is the width at half maximum of the analyzed peaks, and λ is the wavelength of the x rays. From the (022) and (115) reflections of the spinel phase we have estimated a mean crystallite size, $D_{NCFO} \sim 4.6$ nm, which is similar for both samples. Moreover, a mean crystallite size for the CoO cores was estimated from the (002) reflection, and D_{CoO} was found to be 5.0(2) nm and 5.4(2) nm for as-synthesized and annealed samples, respectively. The parameters arising from the structural characterization are summarized in Table I.

TEM micrographs and size-dispersion histograms (obtained by measuring ~250 particles) of as-synthesized and annealed samples are shown in Figs. 2 and 3, respectively. From the lognormal fits of the histograms through the expression $f(D) = (\sqrt{2}\pi\sigma D)^{-1}e^{-\ln^2(D/D_0)/2\sigma^2}$ we have obtained a mean diameter $\langle D\rangle$ of 6.3 and 6.4 nm for as-synthesized and annealed samples, respectively, with a slightly higher size

TABLE I. Summary of the structural characterization of $CoO/Co_{0.5}Ni_{0.5}Fe_2O_4$ nanoparticles: total mean diameter $\langle D \rangle$ and standard deviation σ_D estimated from TEM measurements and mean crystallite size for CoO (D_{CoO}) and $Ni_{0.5}Co_{0.5}Fe_2O_4$ (D_{NCFO}) estimated from XRD experiments (all values are in nm).

	TEM		XRD	
$CoO/Ni_{0.5}Co_{0.5}Fe_2O_4$	$\langle D \rangle$	σ_D	D_{CoO}	D_{NCFO}
As synthesized	6.3	1.0	5.0(2)	4.7(3)
Annealed	6.4	1.2	5.4(2)	4.5(3)

dispersion for the annealed sample, as reflected in the standard deviation calculated by $\sigma_D = \langle D \rangle \sqrt{e^{\sigma^2} - 1}$. Dark-field TEM images, constructed by positioning the objective aperture in the position of the (022) diffraction ring associated with the Ni-Co ferrite, unveil the core/shell structure, as shown in Fig. 3(b). From the TEM analysis it is possible to argue that residual carbon from the synthesis process prevents the agglomeration of the particles. The total mass of the organic material was estimated from the thermogravimetric curves shown in the inset of Fig. 1 and was 63% and 53% for as-synthesized and annealed samples, respectively. It is noteworthy that the organic coating of the nanoparticles is decomposed at higher temperatures compared with pure oleic acid. Such a shift could be due to the stabilization of the oleic acid molecule at the surface of the nanoparticles. In this sense, the decomposition of the residual organic material of the annealed sample is negligible for temperatures below ~300 °C.

On the other hand, a shell thickness of ~1.5 nm was estimated from TEM images. The total volume of the shell can be estimated from the thickness value, which is significantly larger than the crystallite diameter obtained by the XRD analysis. Such a difference is explained by considering a polycrystalline ferrite shell formed by several partially aligned nanograins grown over the CoO cores, as shown in Fig. 2 and suggested by dark-field TEM images; a similar shell

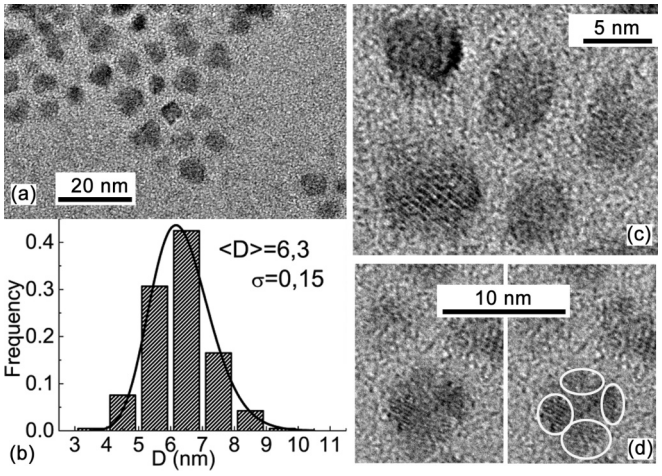

FIG. 2. (a) Bright-field image, (b) size-distribution histogram with the corresponding lognormal fit and (c-d) high-resolution TEM images of as-synthesized $CoO/Co_{0.5}Ni_{0.5}Fe_2O_4$ nanoparticles, where shell nanograins are highlighted.

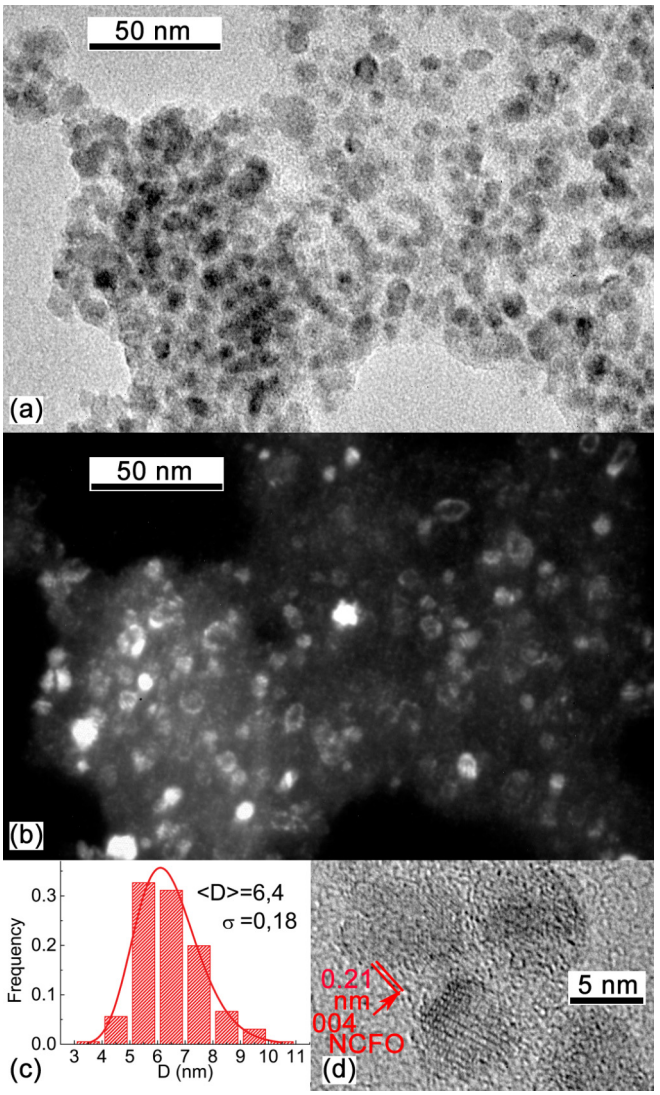

FIG. 3. (a) Bright-field and (b) dark-field TEM images, (c) size-distribution histogram and the corresponding lognormal fit, and (d) high-resolution TEM image of annealed $CoO/Co_{0.5}Ni_{0.5}Fe_2O_4$ nanoparticles.

morphology was also observed in other core/shell nanoparticles [25,30].

Figure 4 shows the ZFC and FC magnetization curves for as-produced nanoparticles, measured applying a field of 50 Oe. Above 270 K the magnetization presents a reversible behavior compatible with the superparamagnetic regime, while at lower temperatures the ZFC-FC curves split according to the progressive blocking of the nanoparticles' magnetic moments. The FC curve increases monotonically when the temperature decreases, while the ZFC curve presents a maximum at $T \sim 100$ K. In addition, a remarkable enhancement of the ZFC magnetization is observed for $T < 15$ K. From the magnetization curves, the energy-barrier distribution $f(T_B)$ was calculated according to $f(T_B) \propto \frac{1}{T} \frac{d(M_{ZFC} - M_{FC})}{dT}$ [31–33]. The mean blocking temperature of as-synthesized nanoparticles, $\langle T_B \rangle = 49$ K, was obtained by fitting $f(T_B)$ with a lognormal function, as shown in the inset of Fig. 4(a). With the aim of studying the dynamics of the magnetic moment,

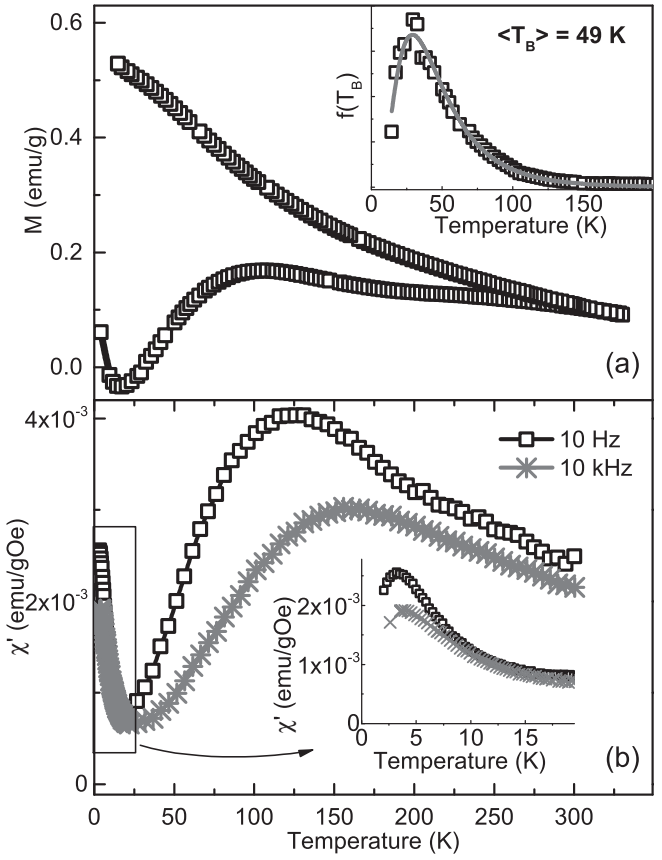

FIG. 4. (a) ZFC and FC dc magnetization curves measured at $H = 50$ Oe [the inset shows the energy-barrier distribution $f(T_B)$ and the corresponding lognormal fit used to estimate $\langle T_B \rangle$] and (b) the real (χ') component of the ac susceptibility measured with $H_{ac} = 10$ Oe at selected frequencies (the inset shows a detail of the low-temperature peak) for as-synthesized $CoO/Co_{0.5}Ni_{0.5}Fe_2O_4$ nanoparticles.

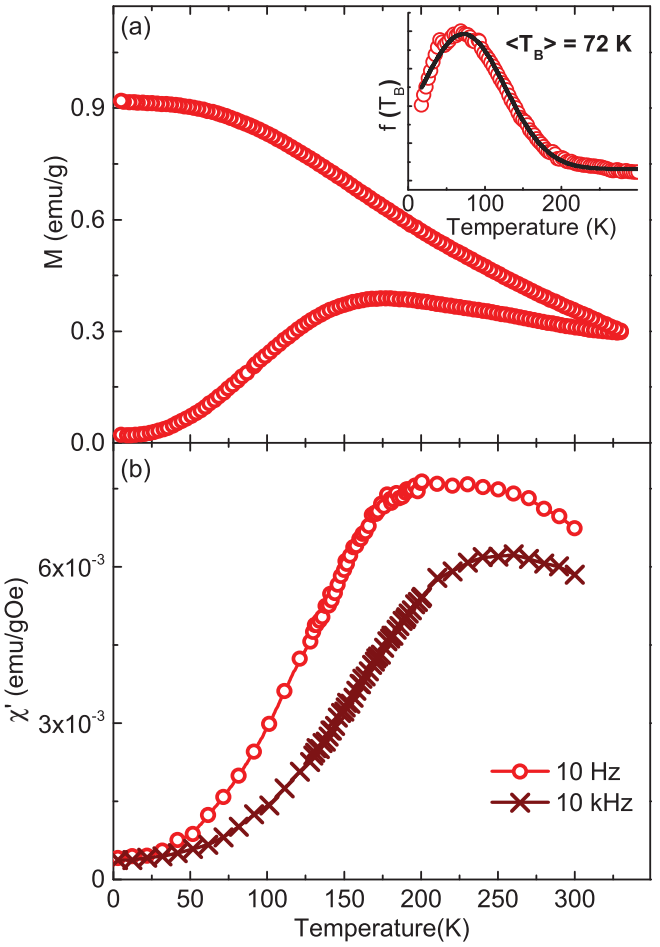

FIG. 5. (a) ZFC and FC dc magnetization curves measured at $H = 50$ Oe [the inset shows the energy-barrier distribution $f(T_B)$ and the corresponding lognormal fit used to estimate $\langle T_B \rangle$] and (b) the real (χ') component of the ac susceptibility measured with $H_{ac} = 10$ Oe at selected frequencies for annealed $CoO/Co_{0.5}Ni_{0.5}Fe_2O_4$ nanoparticles.

ac susceptibility measurements were performed at different frequencies. Figure 4(b) shows the real χ' component of the ac susceptibility for representative frequencies, measured with $H_{ac} = 10$ Oe. The relevant characteristic of these measurements is the presence of two peaks, located at low and high temperatures, with distinct frequency dependence, suggesting a different origin for each maximum. While the χ' maximum at $T \sim 3$ K is slightly frequency dependent, the high-temperature peak is located at about 125 K for $f = 10$ Hz and shifts to about 160 K when the frequency increases to 10 kHz.

The magnetic behavior of the annealed sample is, to some extent, different. Figure 5 shows the temperature dependence of the dc and ac magnetization curves measured at 50 and 10 Oe, respectively. A typical change from the superparamagnetic to blocked regime is observed in the ZFC and FC magnetization curves, where the ZFC maximum is located at a higher temperature ($T \sim 175$ K) compared with as-produced particles. In addition, the FC curve shows a flat behavior at low temperature which evidences the increase of the inter- and intraparticle interactions when the system is annealed. As in the previous case, the mean blocking temperature was calculated by fitting the energy-barrier distribution with a lognormal function, resulting in $\langle T_B \rangle = 72$ K [inset of Fig. 5(a)]. The ac susceptibility of the annealed system shows a single maximum located at about 210 K for $f = 10$ Hz that shifts to about 250 K when the frequency increases to 10 kHz, and there is no evidence of any low-temperature anomaly. Notice that the single peak of the annealed sample, associated with the blocking of the nanoparticles' magnetic moment, is broader and is shifted ~100 K to higher temperatures compared with the as-synthesized system. The larger size dispersion and the presence of enhanced particle interactions, in agreement with the observation of a higher blocking temperature and the FC magnetization behavior, are responsible for such a marked difference.

The blocking process and the collective behavior manifested in the dynamic measurements can be elucidated by analyzing their frequency dependence. The strong frequency dependence of the high-temperature maximum observed for both samples is consistent with a thermally activated hopping of the nanoparticles' magnetic moment over the energy barrier E_a. However, unphysical results were obtained from the fitting with the simple Arrhenius law $\tau = \tau_0 \exp(E_a/k_B T)$, where $\tau = 1/f$ and τ_0 is the characteristic relaxation time of the system. For the as-synthesized sample $E_a/k_B = 3744$ K and

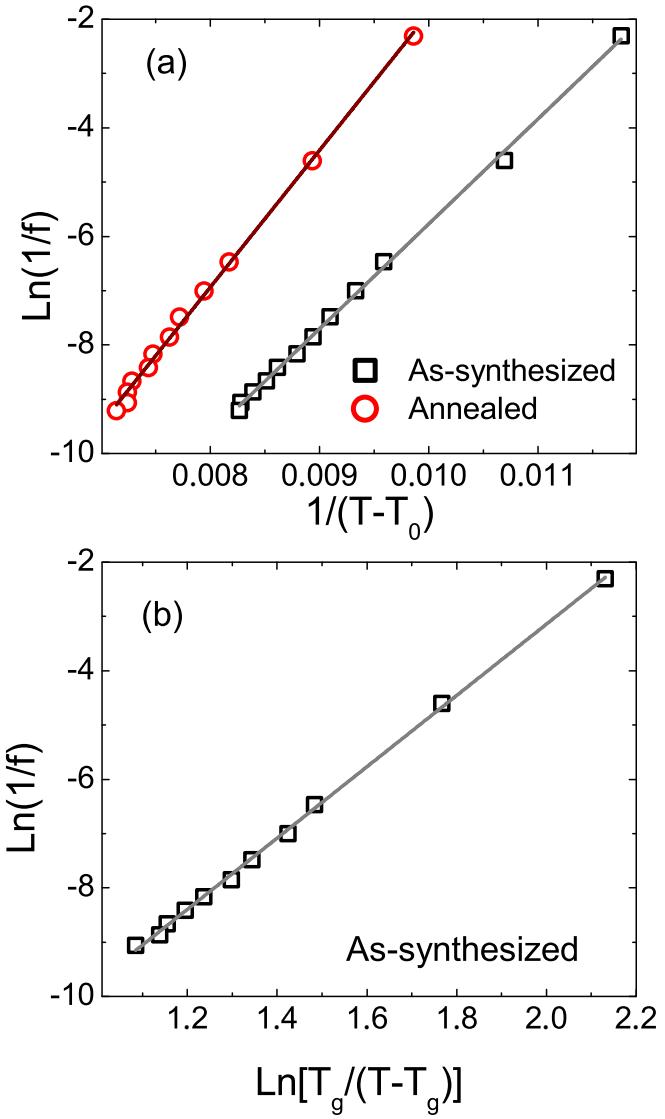

FIG. 6. (a) Frequency dependence of the high-temperature maximum for as-synthesized and annealed nanoparticles. The solid lines correspond to the fit of the experimental data with the Vogel-Fulcher law, Eq. (1). (b) Frequency dependence of the low-temperature maximum for as-synthesized nanoparticles and the corresponding fit with the power law, Eq. (2).

$\tau_0 = 8\times10^{-15}$ s were calculated, where τ_0 is at least three orders of magnitude lower than that expected for ferrimagnetic systems [34], and the parameters obtained for the annealed sample are even farther away from being realistic: $E_a/k_B =$ 9447 K and $\tau_0 = 5\times10^{-21}$ s. This behavior evidences the presence of interactions that affect the relaxation process. Therefore, the frequency dependence of the high-temperature maxima were fitted with a phenomenological Vogel-Fulcher law:

$$\tau = \tau_0 \exp\left(\frac{E_A/k_B}{T - T_0}\right), \tag{1}$$

where T_0 accounts for the weak or moderate effective interactions between the nanoparticles' magnetic moments [35,36]. Figure 6 shows the high-temperature peaks of both samples as a function of the normalized temperature T_0 with the corresponding fitting curve. The parameters obtained from the fitting, reported in Table II, are consistent with the thermally activated process of interacting magnetic moments. The larger T_0 and E_A/k_B values found for the annealed sample are in agreement with the enhancement of the interactions that affect not only T_0 but also the relaxation time and the energy barrier itself. From the adjusted parameters the expected M_{ZFC} peak for the measuring time $t = 100$ s can be obtained. The calculation leads to 105 and 191 K for the as-synthesized and the annealed samples, respectively, close to the maxima of the dc magnetization curves, confirming good agreement between both measurements.

The frequency dependence of the low-temperature peak for as-synthesized nanoparticles shows, in contrast, a much slower dynamics. As a consequence, neither Arrhenius's law nor the Vogel-Fulcher law yields physically reasonable results, and the dynamic behavior of the magnetic susceptibility in this range of temperature would not be associated with a thermally activated process of individual or weakly interacting particle moments. Instead, a collective freezing mechanism, with a standard critical slowing-down dependence [37], should be the origin of the low-temperature peak that follows a power law according to

$$\tau = \tau_0\left(\frac{T_g}{T - T_g}\right)^{z\nu}, \tag{2}$$

where T_g is the static freezing temperature, ν is the critical exponent of the correlation length, and z is the dynamic exponent. From the fitting using Eq. (2) we obtained $T_g = 3.0$ K, $z\nu = 6.6$, and $\tau_0 = 1.3\times10^{-8}$ s. While $z\nu$ is in agreement with the usual values found for the critical exponent of spin glasses ($z\nu = 6-9$), the relaxation time seems to be larger, although it is in agreement with the values reported for some cluster spin-glass and superspin-glass systems [38–43].

The frequency and temperature dependence of the magnetization for as-produced nanoparticles gives an overall picture of the core/shell system: the magnetic moments of the

TABLE II. Summary results of the dc and ac measurements: mean blocking temperature $\langle T_B \rangle$, coercivity at 10 K H_C, exchange-bias field at 10 K H_{EB}, and parameters calculated from the Vogel-Fulcher model for the high-temperature χ' peaks and from the power-law model for the low-temperature χ' peaks.

				Vogel-Fulcher (high T)			Power law (low T)		
$CoO/Ni_{0.5}Co_{0.5}Fe_2O_4$	$\langle T_B \rangle$ (K)	H_C (kOe)	H_{EB} (kOe)	τ_0 (s)	T_0 (K)	E/k_B (K)	τ_0 (s)	T_g (K)	$z\nu$
As synthesized	49	5.5	0.8	1.3×10^{-11}	40(12)	1933(23)	8.5×10^{-8}	3.0(1)	6.6(1)
Annealed	72	14.6	2.3	1.7×10^{-12}	112(23)	2514(40)			

interacting nanoaggregates of spins that constitute the highly disordered ferrimagnetic shell are superparamagnetic at room temperature and block at $\langle T_B \rangle = 49$ K. When the temperature decreases, the thermal fluctuations slow down, the short-range magnetic correlations increase, and the magnetic moments of the nanoaggregates of the shell randomly freeze at T $\sim$ 3 K. In the case of the annealed sample, the thermal stability of the magnetic moment increases, and as a consequence, the blocking temperature is almost doubled. The blocking temperature can be compared with the reported values for Ni-substituted cobalt ferrite single-phase nanoparticles. Maaz *et al.* found a M_{ZFC} maximum at around 170 K for 12-nm $Co_{0.7}Ni_{0.3}Fe_2O_4$ nanoparticles [44], and a M_{ZFC} maximum of around 120 K was observed for (6.6 ± 1.0)-nm $Co_{0.42}Ni_{0.56}Fe_2O_4$ nanoparticles [45], reflecting the increased thermal stability of our system, where the average ferrite shell thickness is $\sim$1.5 nm. The enhancement of the thermal stability of the core/shell system compared to a spinel single-phase nanoparticle is associated with the interfacial AFM/FiM exchange couplings, which, in the annealed system, are stronger as a consequence of the increasing degree of crystalline order of the CoO phase, as shown by the XRD experiments. Even if these experimental results sketch the dynamics of the nanoparticle magnetic moments, they do not provide details of the role of the intraparticle interactions. Therefore, with the aim of elucidating the role of the AFM/FiM coupling, the field dependence of the magnetization was investigated.

From the ZFC and FC hysteresis loops presented in Fig. 7 (the latter measured after cooling the sample from 320 K at an applied field of 10 kOe), the coercivity $H_C = (H_C^+ - H_C^-)/2$ and exchange bias shift $H_{EB} = (H_C^+ + H_C^-)/2$ were calculated. Several interesting features can be noted from the loops. The most noticeable one is the enhancement of the coercive field when the sample is annealed: at 10 K, $H_C \sim 5.5$ kOe and $\sim$14.6 kOe for as-prepared and annealed nanoparticles, respectively. The enhancement of H_C in the annealed sample is even more evident when it is compared with $Co_{0.5}Ni_{0.5}Fe_2O_4$ single-phase nanoparticles, whose H_C is, for example, $\sim$6 and $\sim$12 kOe for 7.6- and 22-nm nanoparticles [46,47], respectively. While the coercivity of annealed nanoparticles increases monotonically as the temperature is decreased, H_C diminishes below 14 K for as-synthesized nanoparticles, as shown in Fig. 8. Nonmonotonous dependence of the coercive field could be associated with the magnetic frustration due to the increase in the magnetic correlation of surface spins or due to intra- or interparticle interactions [38,48–50]. Both samples present exchange-bias field, consistent with the presence of interface exchange coupling between the hard-AFM and the soft-FiM phases. However, the exchange-bias field is almost 3 times higher for the annealed sample. It is worth noting that, although in ideal systems the exchange-bias properties are expected to be observed up to the Néel temperature, in many nanostructures the effect disappears at temperatures much lower than T_N [51]. Finite-size effects, associated with the decrease of the anisotropy energy of the CoO, could be responsible for such an effect; in fact, if the core is small enough, the AFM anisotropy could fail to pin the FiM spins either as a result of its superparamagnetic relaxation or because the magnetic moments are reversed by the rotation of the FiM moment itself [52]. On the other hand, the interactions modify

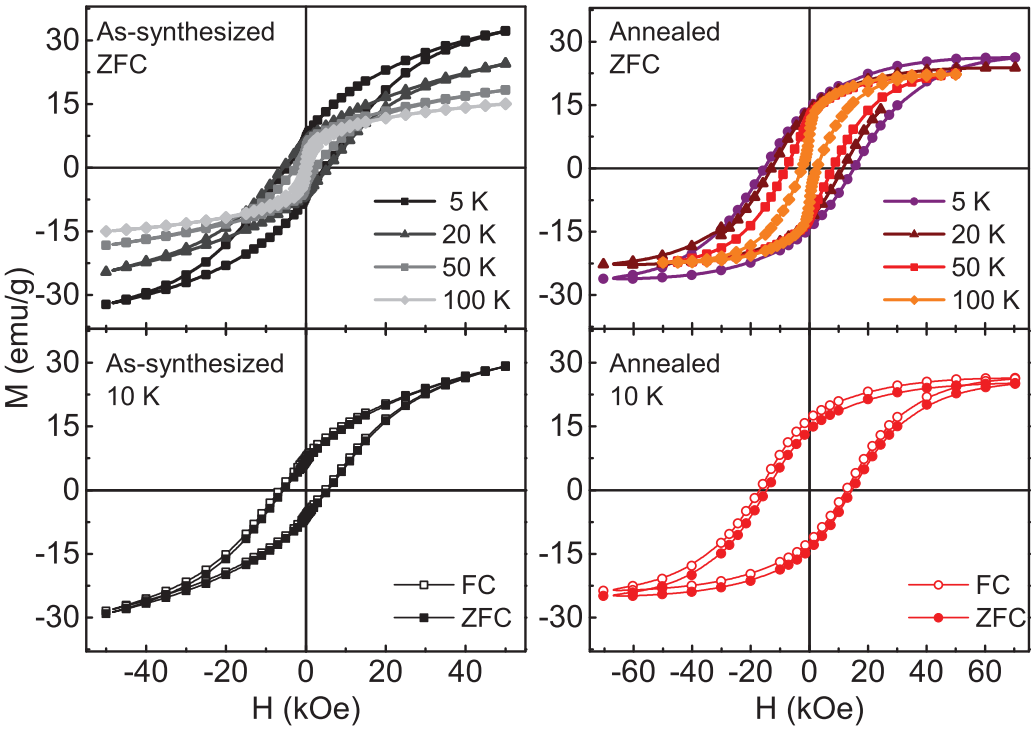

FIG. 7. ZFC hysteresis cycles for several temperatures and FC hysteresis curves at 10 K for as-synthesized and annealed $CoO/Ni_{0.5}Co_{0.5}Fe_2O_4$ nanoparticles.

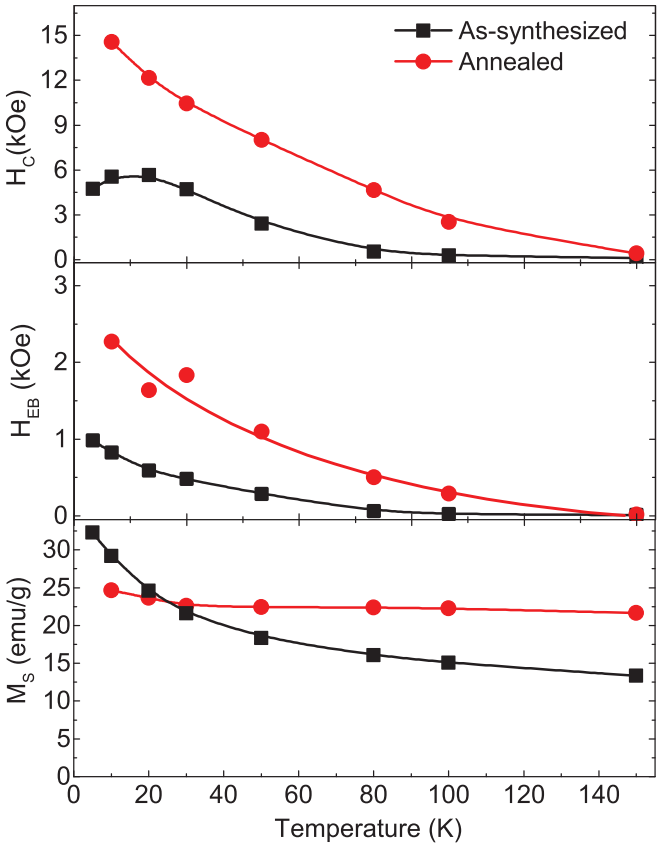

FIG. 8. Temperature dependence of the coercive field H_C, the exchange-bias field H_{EB}, and the saturation magnetization M_S for as-synthesized and annealed $CoO/Ni_{0.5}Co_{0.5}Fe_2O_4$ nanoparticles.

the energy-barrier distribution [31] $f(T_B)$, which strongly depends on the interface quality and the interface exchange coupling. Therefore, although the nanoparticle system presents a narrow size distribution, $f(T_B)$ is expected to be wider in bimagnetic nanoparticles due to local variations of the anisotropy and interface interactions and the possibility of core-shell intermixing [53]. As a consequence, H_C and H_{EB} are observed up to much higher temperatures than $\langle T_B \rangle$, i.e., 100 and 150 K for the as-synthesized and annealed particles, respectively. The possibility of core-shell interdiffusion in the annealed sample [19,53], suggested by the large dispersion of energy barriers, could be an important factor to control the magnitude of H_{EB} and H_C. In this sense, further systematic studies of the interface composition in as-synthesized and annealed samples are needed to clarify such a still scarcely studied feature of bimagnetic heterostructures. Finally, notice that the saturation magnetization M_S of the as-synthesized sample presents an important increase as the temperature diminishes, while M_S of the annealed sample remains almost unchanged.

The larger H_{EB} values for the annealed sample indicate a stronger pinning action exerted by the AFM phase on the moments of the FiM one. This is due to the increase of the anisotropy with the increase of CoO crystallinity after annealing, but the enhancement of the coercive field also demonstrates that a fraction of the spins belonging to the AFM core can be dragged by the FiM shell. These effects are barely noticeable in the as-prepared samples due to lower crystallinity of CoO, with the consequent lower density of exchange interaction bonds through the FiM/AFM interface. Therefore, the magnetic behavior of the as-synthesized sample is similar to that observed in hollow ferrimagnetic nanoparticles, where the shell is formed by superparamagnetic interacting nanocrystals. The interplay between the interacting shell nanocrystals and the intrinsic disorder of this system, due to the magnetic and crystalline disorder and different orientations of anisotropy axes of the shell nanocrystals, leads to frustration and development of collective freezing at low temperatures [40,54].

IV. CONCLUSIONS

It was shown that the surface and crystalline order/disorder determine the static and dynamic behavior of bimagnetic CoO-core/$Co_{0.5}Ni_{0.5}Fe_2O_4$-shell nanoparticles. The disorder degree, and, consequently, the magnetic properties of the nanoparticles systems under investigation, can be controlled by thermal treatments. At room temperature, the core/shell nanoparticles show a superparamagnetic behavior. The magnetic moment of the annealed sample is 50% larger than that of the as-synthesized sample, evidencing an important fraction of magnetically disordered FiM shell in the latter one. When the temperature decreases, the magnetic moments of as-synthesized nanoparticles progressively block, the magnetic correlation increases, and the system freezes into a superspin-glass state at very low temperature. The blocking of interacting particle moments and the collective freezing were well evidenced by the thermal activation process and critical slowing-down behavior, respectively, determined by dynamic ac susceptibility measurements. On the other hand, the AFM/FiM interface coupling was confirmed by the presence of exchange bias. The interface coupling is reinforced for the annealed sample due to the increase of the density of exchange bonds at the interface as a consequence of the increased degree of crystalline order in CoO. Annealed $CoO/Co_{0.5}Ni_{0.5}Fe_2O_4$ thus has larger values of coercive fields and exchange bias fields [$H_C(10K) \sim 14.6$ kOe, $H_{EB}(10K) \sim 2.3$ kOe] compared with single-phase counterparts. Notice that even if from a basic crystalline and morphological characterization both samples exhibit similar size, morphology, and crystalline phases, the magnetic behavior of the as-synthesized nanoparticles resembles that reported for hollow ferrites, in which the large surface disorder governs the magnetic properties, while the behavior of the annealed system is driven by the AFM/FiM interface coupling.

ACKNOWLEDGMENTS

The authors thank ANPCyT Argentine for support through Grant No. PICT-2012-0492, CONICET Argentina for support through Grant No. PIP 112-20110100519, and UNCuyo for support through Grant No. C011.

[1] A. López-Ortega, M. Estrader, G. Salazar-Alvarez, A. G. Roca, and J. Nogués, Phys. Rep. **553**, 1 (2015).

[2] B. Balamurugan, D. Sellmyer, G. Hadjipanayis, and R. Skomski, Scr. Mater. **67**, 542 (2012).

[3] E. L. Winkler, E. Lima, D. Tobia, M. E. Saleta, H. E. Troiani, E. Agostinelli, D. Fiorani, and R. D. Zysler, Appl. Phys. Lett. **101**, 252405 (2012).

[4] G. Muscas, P. Anil Kumar, G. Barucca, G. Concas, G. Varvaro, R. Mathieu, and D. Peddis, Nanoscale **8**, 2081 (2016).

[5] B. Balasubramanian, B. Das, R. Skomski, W. Y. Zhang, and D. J. Sellmyer, Adv. Mater. **25**, 6090 (2013).

[6] C. N. Chinnasamy, M. Senoue, B. Jeyadevan, O. Perales-Perez, K. Shinoda, and K. Tohji, J. Colloid Interface Sci. **263**, 80 (2003).

[7] V. Skumryev, S. Stoyanov, Y. Zhang, G. Hadjipanayis, D. Givord, and J. Nogués, Nature (London) **423**, 850 (2003).

[8] A. K. Gupta and M. Gupta, Biomaterials **26**, 3995 (2005).

[9] J.-H. Lee, J.-T. Jang, J.-S. Choi, S. H. Moon, S.-H. Noh, J.-W. Kim, J.-G. Kim, I.-S. Kim, K. I. Park, and J. Cheon, Nat. Nanotechnol. **6**, 418 (2011).

[10] V. Mameli, A. Musinu, A. Ardu, G. Ennas, D. Peddis, D. Niznansky, C. Sangregorio, C. Innocenti, N. T. K. Thanh, and C. Cannas, Nanoscale **8**, 10124 (2016).

[11] H. Zeng, J. Li, Z. L. Wang, J. P. Liu, and S. Sun, Nano Lett. **4**, 187 (2004).

[12] G. C. Lavorato, E. Lima. Jr., D. Tobia, D. Fiorani, H. E. Troiani, R. D. Zysler, and E. L. Winkler, Nanotechnology **25**, 355704 (2014).

[13] F. Liu, J. Zhu, W. Yang, Y. Dong, Y. Hou, C. Zhang, H. Yin, and S. Sun, Angew. Chem., Int. Ed. **53**, 2176 (2014).

[14] J. Nogués, V. Skumryev, J. Sort, S. Stoyanov, and D. Givord, Phys. Rev. Lett. **97**, 157203 (2006).

[15] D. W. Kavich, J. H. Dickerson, S. V. Mahajan, S. A. Hasan, and J.-H. Park, Phys. Rev. B **78**, 174414 (2008).

[16] G. Salazar-Alvarez, J. Sort, S. Surinach, M. D. Baró, and J. Nogués, J. Am. Chem. Soc. **129**, 9102 (2007).

[17] A. E. Berkowitz, G. F. Rodriguez, J. I. Hong, K. An, T. Hyeon, N. Agarwal, D. J. Smith, and E. E. Fullerton, Phys. Rev. B **77**, 024403 (2008).

[18] K. L. Krycka, J. A. Borchers, G. Salazar-Alvarez, A. López-Ortega, M. Estrader, S. Estradé, E. Winkler, R. D. Zysler, J. Sort, F. Peiró *et al.*, ACS Nano **7**, 921 (2013).

[19] S. Estradé, L. Yedra, A. Lopez-Ortega, M. Estrader, G. Salazar-Alvarez, M. Baro, J. Nogues, and F. Peiro, Micron **43**, 30 (2012).

[20] M. Estrader, A. López-Ortega, I. V. Golosovsky, S. Estradé, A. G. Roca, G. Salazar-Alvarez, L. López-Conesa, D. Tobia, E. Winkler, J. D. Ardisson *et al.*, Nanoscale **7**, 3002 (2015).

[21] A. López-Ortega, D. Tobia, E. Winkler, I. V. Golosovsky, G. Salazar-Alvarez, S. Estradé, M. Estrader, J. Sort, M. A. González, S. Surinach *et al.*, J. Am. Chem. Soc. **132**, 9398 (2010).

[22] G. Muscas, G. Concas, C. Cannas, A. Musinu, A. Ardu, F. Orrù, D. Fiorani, S. Laureti, D. Rinaldi, G. Piccaluga *et al.*, J. Phys. Chem. C **117**, 23378 (2013).

[23] M. Qureshi, S. Baker, C. Binns, M. Roy, S. Laureti, D. Fiorani, and D. Peddis, J. Magn. Magn. Mater. **378**, 345 (2015).

[24] M. Vasilakaki, K. N. Trohidou, and J. Nogués, Sci. Rep. **5**, 9609 (2015).

[25] E. Lima, E. L. Winkler, D. Tobia, H. E. Troiani, R. D. Zysler, E. Agostinelli, and D. Fiorani, Chem. Mater. **24**, 512 (2012).

[26] G. C. Lavorato, E. Lima, H. E. Troiani, R. D. Zysler, and E. L. Winkler, J. Alloys Compd. **633**, 333 (2015).

[27] E. Lottini, A. López-Ortega, G. Bertoni, S. Turner, M. Meledina, G. Van Tendeloo, C. J. Fernández, and C. Sangregorio, Chem. Mater. **28**, 4214 (2016).

[28] M. Estrader, A. López-Ortega, S. Estradé, I. V. Golosovsky, G. Salazar-Alvarez, M. Vasilakaki, K. N. Trohidou, M. Varela, D. C. Stanley, M. Sinko *et al.*, Nat. Commun. **4**, 2960 (2013).

[29] J. M. Coey, *Magnetism and Magnetic Materials* (Cambridge University Press, Cambridge, 2010).

[30] X. Liu, B. P. Pichon, C. Ulhaq, C. Lefèvre, J.-M. Grenèche, D. Bégin, and S. Bégin-Colin, Chem. Mater. **27**, 4073 (2015).

[31] J. Dormann, D. Fiorani, and E. Tronc, *Magnetic Relaxation in Fine-Particle Systems*, Advances in Chemical Physics Vol. 98 (Wiley, New York, 1997).

[32] R. Chantrell, M. El-Hilo, and K. O'Grady, IEEE Trans. Magn. **27**, 3570 (1991).

[33] M. Knobel, W. C. Nunes, L. M. Socolovsky, E. De Biasi, J. M. Vargas, and J. C. Denardin, J. Nanosci. Nanotechnol. **8**, 2836 (2008).

[34] E. Lima, E. De Biasi, M. V. Mansilla, M. E. Saleta, F. Effenberg, L. M. Rossi, R. Cohen, H. R. Rechenberg, and R. D. Zysler, J. Appl. Phys. **108**, 103919 (2010).

[35] S. Shtrikman and E. P. Wohlfarth, Phys. Lett. A **85**, 467 (1981).

[36] D. Peddis, C. Cannas, A. Musinu, A. Ardu, F. Orrù, D. Fiorani, S. Laureti, D. Rinaldi, G. Muscas, G. Concas *et al.*, Chem. Mater. **25**, 2005 (2013).

[37] K. Binder and A. P. Young, Rev. Mod. Phys. **58**, 801 (1986).

[38] P. Gorria, A. B. Fuertes, L. F. Barquin, and J. A. Blanco, Nanotechnology **26**, 305705 (2015).

[39] H. Khurshid, P. Lampen-Kelley, Ò. Iglesias, J. Alonso, M.-H. Phan, C.-J. Sun, M.-L. Saboungi, and H. Srikanth, Sci. Rep. **5**, 15054 (2015).

[40] S. Chandra, H. Khurshid, W. Li, G. C. Hadjipanayis, M. H. Phan, and H. Srikanth, Phys. Rev. B **86**, 014426 (2012).

[41] C. Djurberg, P. Svedlindh, P. Nordblad, M. F. Hansen, F. Bodker, and S. Morup, Phys. Rev. Lett. **79**, 5154 (1997).

[42] W. Kleemann, O. Petracic, C. Binek, G. N. Kakazei, Y. G. Pogorelov, J. B. Sousa, S. Cardoso, and P. P. Freitas, Phys. Rev. B **63**, 134423 (2001).

[43] D. Peddis, D. Rinaldi, G. Ennas, A. Scano, E. Agostinelli, and D. Fiorani, Phys. Chem. Chem. Phys. **14**, 3162 (2012).

[44] K. Maaz, S. Karim, and G.-H. Kim, Chem. Phys. Lett. **549**, 67 (2012).

[45] T. Orlando, M. Albino, F. Orsini, C. Innocenti, M. Basini, P. Arosio, C. Sangregorio, M. Corti, and A. Lascialfari, J. Appl. Phys. **119**, 134301 (2016).

[46] S. Kubickova, J. Vejpravova, P. Holec, and D. Niznansky, J. Magn. Magn. Mater. **334**, 102 (2013).

[47] H. M. Abdallah, T. Moyo, and N. Ngema, J. Magn. Magn. Mater. **394**, 223 (2015).

[48] E. Winkler, R. D. Zysler, M. V. Mansilla, and D. Fiorani, Phys. Rev. B **72**, 132409 (2005).

[49] E. Winkler, R. D. Zysler, M. Vasquez Mansilla, D. Fiorani, D. Rinaldi, M. Vasilakaki, and K. N. Trohidou, Nanotechnology **19**, 185702 (2008).

[50] R. D. Zysler, D. Fiorani, and A. M. Testa, J. Magn. Magn. Mater. **224**, 5 (2001).

[51] J. Nogués, J. Sort, V. Langlais, V. Skumryev, S. Surinach, J. Munoz, and M. Baró, Phys. Rep. **422**, 65 (2005).

[52] J. B. Tracy, D. N. Weiss, D. P. Dinega, and M. G. Bawendi, Phys. Rev. B **72**, 064404 (2005).

[53] E. Skoropata, R. D. Desautels, C.-C. Chi, H. Ouyang, J. W. Freeland, and J. van Lierop, Phys. Rev. B **89**, 024410 (2014).

[54] K. Hiroi, K. Komatsu, and T. Sato, Phys. Rev. B **83**, 224423 (2011).